Stark shift and width of x-ray lines from highly charged ions in dense plasmas

M. F. Gu and P. Beiersdorfer
Space Science Laboratory, University of California, Berkeley, California 94720, USA

We implement several plasma screening potentials to calculate the level energy shifts of highly charged ions in warm dense plasmas. The Stark widths of transitions are treated with an empirical interpolation scheme combining the impact approximation and the quasicontiguous approximation. The resulting shift-width relationship is compared with recent experimental measurements of the $K\beta$ transition of He-like Cl from the Orion laser facility.

I. INTRODUCTION

Atomic data needed to describe the emission and absorption of radiation from highly charged ions embedded in a plasma are typically calculated in the isolated-atom approximation, in which perturbing effects from the surrounding ions are neglected. This is generally a good approximation for coronal plasmas and many low-density laboratory plasmas, such as those produced in tokamaks and other magnetic confinement devices. As the density increases, however, plasma effects start to noticeably affect the atomic parameters. In particular, the central nuclear field that determines the atomic properties of an isolated ion is modified by the fields of neighboring ions and closely packed free plasma electrons. The resulting effects can significantly change atomic properties, and express themselves, for example, as ionization potential depression, the vanishing of spectral lines from higher-lying atomic levels, the broadening of spectral lines, and the change in the position of the emitted lines [1–6].

The importance of high-density effects is now being recognized for the radiative properties of accretion disks surrounding black holes as well as for the radiation transport and opacity of stellar interiors [7,8]. Field-induced spectral line broadening has also been recognized as an important diagnostic tool for inferring the density of laboratory plasmas, e.g., those produced in inertial confinement fusion experiments, and this effect has been observed in a variety of laboratory plasmas [9–11].

Recent experimental observations of dense plasma line shifts open up the possibility of determining the plasma density from high-resolution spectral measurements of spectral line positions. Line broadening measurements used for inferring the plasma density are affected by systematic and instrumental effects, such as by assumptions of the level of the radiative background in a given spectrum. Such systematic uncertainties are absent in line-shift determinations, and thus they offer an alternative and complementary method that potentially has higher accuracy—provided that the underlying theory of dense plasma line shifts is well understood. However, there are still significant disagreements among the theoretical models that describe field-induced line shifts. For

example, a recent measurement of both shift and width of the $K\beta$ transition of He-like Cl from the Orion laser facility indicated significant disagreement with existing theoretical models [12]. Specifically, it was shown that the recent theoretical line-shift model of Li and Rosmej [13] overestimated the energy shift by about a factor of 2 at electron densities that are inferred from the linewidths according to the standard theory of Stark broadening. Clearly, additional theoretical developments are needed to put a potential density diagnostic based on line shifts on a solid footing and, of course, to provide reliable atomic data for the modeling of the radiative properties of astrophysical and laboratory plasmas.

In the present paper, we implement a detailed numerical line-shift model in the framework of the flexible atomic code (FAC) of Gu [14], and develop an efficient method for determining Stark widths of transitions from complex ions. Various forms of screening potentials have been employed in the past to address the lowering of the continuum and shifting of spectral lines; some of them have also been implemented in FAC and other widely used atomic structure codes [15,16]. The most popular models are the Debye-Hückel and ion sphere potentials, which are valid in two opposite regimes of plasma conditions. In the present paper, we also implement the screening potential based on the model proposed by Stewart and Pyatt [17], which is expected to work in a wider range of plasma temperature and density parameters. Our empirical method for estimating Stark broadening combines the distorted-wave calculation of electron impact width and the quasicontiguous approximation of Stambulchik and Maron [18]. Significant attention is devoted to account for the effects of strong plasma coupling. To this end, we propose an improved analytical fit of realistic ion microfield distributions based on the work of Potekhin *et al.* [19]. The resulting shifts and widths for the He-like Cl $K\beta$ transition agree well with the Orion measurements.

The paper is organized as follows: Sec. II describes the numerical model of line shifts and its implementation in FAC; Sec. III introduces the empirical model of Stark broadening combining the impact and quasicontiguous approximation; Sec. IV compares the theoretical shifts and widths of the He-like Cl $K\beta$ line with Orion measurements.

II. STARK SHIFT

The shift of energy levels of ions embedded in a warm dense plasma is often treated with screening potentials. In the mean-field approximation, the central potential of an ionic system is written as

$$V(r) = V_0(r) + V_f(r), \quad (1)$$

where $V_0(r)$ is the potential of an isolated ion, while $V_f(r)$ accounts for the screening of free electrons and ions in the plasma. Several forms of the screening potential $V_f(r)$ are widely used, which are valid under different physical conditions. The simplest form is the Debye-Hückel potential. After subtracting $V_0(r)$, we obtain $V_f(r)$ as

$$V_f(r) = V_0(r)\left(e^{-\frac{r}{R_d}} - 1\right), \quad (2)$$

where R_d denotes the Debye screening lengths due to both electrons and ions, the exact definition of which will be given later; note that instead of taking into account the screening of the interelectronic Coulomb interactions and the nuclear potential separately we are using the screening of the total mean potential generated by the nucleus and the bound electrons. This is valid when the Debye length is much larger than the size of the ionic system, which is generally where the Debye screening model can be justified, i.e., in the limit of low density and high temperature. Under this assumption, we can simplify Equation 2 by approximating $V_0(r) = -\frac{z}{r}$, where $z = Z - N_b + 1$ is the residual charge of the ion, Z is the nucleus charge, and N_b is the number of bound electrons.

In the opposite limit of high density and low temperature, the ion sphere model is often employed [20]:

$$V_f(r) = 4\pi\left[\frac{1}{r}\int_0^r r' + \int_r^{R_s}\right]r'\rho_f(r')dr', \quad (3)$$

where $\rho_f(r)$ is the radial distribution of the free electrons in the ion sphere of radius $R_s = [3(Z - N_b)/4\pi n_e]^{1/3}$. The local free-electron densities are assumed to follow the Fermi-Dirac distribution as

$$\rho_f(r) = \frac{1}{\pi^2}\int_{\kappa_0}^\infty \frac{\kappa\, d\kappa}{e^{[\sqrt{\kappa^2 c^2 + c^4} - c^2 + V(r) - \mu]/kT} + 1}, \quad (4)$$

where c is the speed of light, $\kappa_0 = \sqrt{-2V(r)c^2 + V(r)^2}$, and $V(r)$ is the total potential experienced by the free electron. The chemical potential μ is implicitly defined through the charge neutrality condition inside the sphere:

$$4\pi\int_0^{R_s} r^2\rho_f(r)dr = Z - N_b. \quad (5)$$

Note that in this model only the screening by electrons is taken into account. When the temperature is high enough, this screening potential reduces to that of a uniformly distributed electron sphere:

$$V_f(r) = \frac{Z - N_b}{2R_s}\left[3 - \left(\frac{r}{R_s}\right)^2\right]. \quad (6)$$

The ion sphere and Debye-Hückel screening models are valid under different physical conditions. The ion sphere model is valid where $R_d \ll R_s$, while the Debye-Hückel model applies when $R_d \gg R_s$. In the intermediate regime

where $R_d \sim R_s$, both models fail. The screening potential proposed by the Stewart-Pyatt model naturally interpolates the two limits, and is considered to be more accurate [17]. The potential induced by the free electrons is defined by a second-order differential equation based on the Thomas-Fermi model. The equations are often expressed in dimensionless form in terms of $v(x) = V_f(r)/kT$, $y(x) = V(r)/kT$, and $x = r/R_d$, where the total Debye length is defined by

$$\frac{1}{R_d^2} = \frac{4\pi e^2}{kT}(z^* + 1)n_e, \quad (7)$$

where n_e is the electron density far away from the ion, and $z^* = \langle z^2\rangle/\langle z\rangle$ is the ratio of the second and first moments of the ionic charge of a multicomponent plasma.

$y(x)$ is the solution of

$$\frac{1}{x}\frac{d^2}{dx^2}(xy) = \frac{1}{z^* + 1}\left[\frac{F(y - \alpha)}{F(-\alpha)} - e^{-z^* y}\right], \quad (8)$$

where

$$F(y) = \int_0^\infty \frac{t^{1/2}dt}{e^{t-y} + 1}, \quad (9)$$

and the constant α is related to the electron density, n_e, far from the ion:

$$n_e = \frac{2(2\pi mkT)^{3/2}}{h^3}\frac{2}{\sqrt{\pi}}F(-\alpha). \quad (10)$$

$y(x)$ satisfies the boundary conditions $y(\infty) = 0$, and $xy = Ze^2/(R_d kT)$ at the origin.

$v(x)$ is the solution of

$$\frac{1}{x}\frac{d^2}{dx^2}(xv) = \frac{1}{z^* + 1}\left[\frac{F(y - \alpha, y)}{F(-\alpha)} - e^{-z^* y}\right], \quad (11)$$

where

$$F(y - \alpha, y) = \int_y^\infty \frac{t^{1/2}dt}{e^{t+\alpha-y} + 1}. \quad (12)$$

The boundary condition for this second-order differential equation is $dv/dx = 0$ at the origin, and $v(\infty) = 0$.

The three forms of screening potentials discussed above have been implemented in the FAC of Gu [14]. The plasma effects on the atomic structure and on various collisional and radiative data can then be explored in great detail. As an example, Fig. 1 shows the lowering of the ground-state ionization energy of He-like Ar at an electron density of 10^{23} cm^{-3} and as a function of temperature. At this density and with $z^* = 16$, $R_s = R_d$ at the temperature of 3.6 keV. It is seen that the ionization energy shift from the Stewart-Pyatt model approaches the ion sphere limit at low temperatures (large R_s/R_d), and approaches the Debye-Hückel limit at high temperatures (small R_s/R_d).

Figure 2 shows the redshift of the He-like Ar $K\beta$ transition at the same electron density and temperature range. It is interesting to note that, in contrast to the ionization energy lowering, the ion sphere and Stewart-Pyatt models result in very close energy shifts for the $K\beta$ line over a wide temperature range. The Debye-Hückel model performs rather poorly, and is likely only valid at very large R_s/R_d values. This indicates that if one is primarily concerned with the
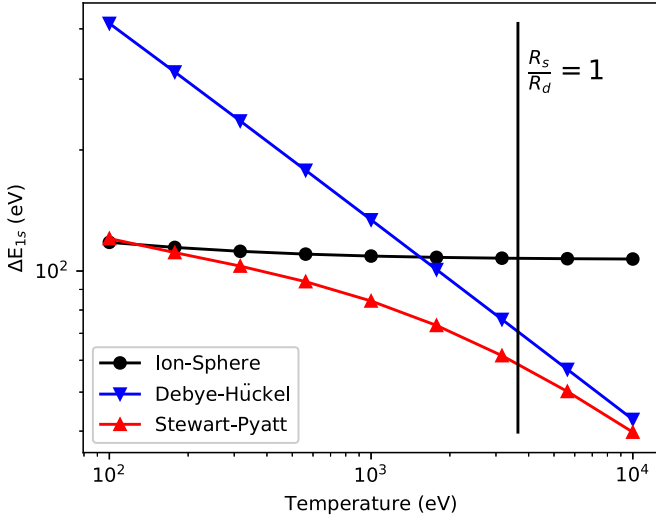
FIG. 1. Lowering of the ground-state ionization energy of He-like Ar at $n_e = 10^{23}$ cm^{-3}. The vertical line represents the temperature where $R_s = R_d$.

shift of transition lines the ion sphere model is a reasonable approximation.

III. STARK WIDTH

The theory of Stark width varies greatly in the level of complexity. For isolated lines and at low densities, the electron is often the dominant perturber, and the impact approximation is valid, such that the Stark broadened line shape is Lorentzian and the full width at half maximum is reduced to the calculation of the elastic and inelastic scattering of electrons from the lower and upper states of the transition lines [21]. For overlapping lines, and when ions contribute significantly to the broadening, the line shapes become more complex, especially when ion dynamic effects cannot be ignored. In such cases, detailed calculations combining the molecular dynamics simulations for ion microfield distribution and the standard
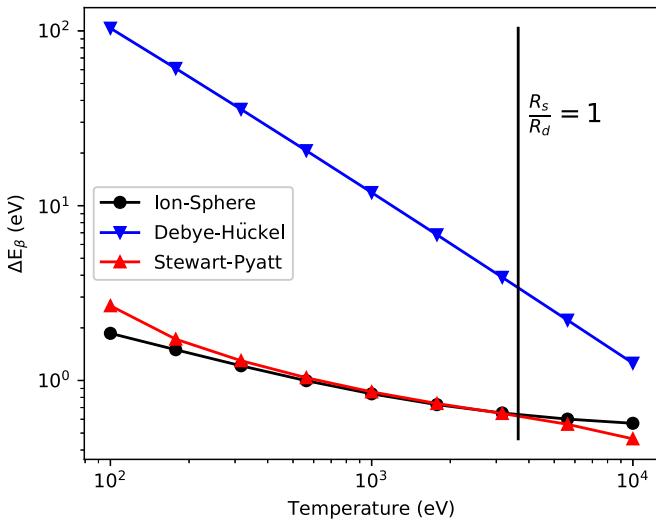

FIG. 2. Redshift of the $K\beta$ transition He-like Ar at $n_e = 10^{23}$ cm^{-3}. The vertical line represents the temperature where $R_s = R_d$.

line-shape theory must be employed. In this paper, we develop a fast yet reasonably accurate method for estimating Stark linewidths, that is suitable for use in large scale, nonlocal thermodynamic equilibrium, collisional radiative models.

Our method starts with the electron impact width calculated with the Baranger formula, w_i^e. The Stark width due to an ion perturber in the impact approximation is then estimated as $w_i^i = z_i \sqrt{m_i} w_i^e$, where z_i and m_i are the charge and reduced mass of the perturbing ion. The scaling factors account for the larger interaction and slower motion of the ions relative to the electrons. However, the impact approximation is generally not valid at high densities. This is especially so for ion perturbers. Therefore, we introduce an empirical interpolation procedure to reproduce the proper density scaling of the linewidth in the quasistatic regime, by combining the impact approximation and the quasicontiguous approximation of Stambulchik and Maron [18]:

$$w_{QC} = w_{QS}\left(\frac{R_0}{R} + 1\right)^{-1}, \qquad (13)$$

where w_{QS} is the quasistatic width, R_0 is an empirical constant of order unity, and $R = w_{QS}/w_{dyn}$. The dynamic width w_{dyn} is given by

$$w_{dyn} = \sqrt{\frac{T}{m_p}}\left(\frac{4\pi}{3}n_p\right)^{1/3}, \qquad (14)$$

where m_p and n_p are the reduced mass and density of the perturber. The quasistatic width w_{QS} has an $n_p^{2/3}$ density dependence, so that at low densities w_{QC} reduces to the impact approximation:

$$w_i = \frac{w_{QS}^2}{R_0 w_{dyn}}. \qquad (15)$$

Using the impact width calculated with the Baranger formula, we determine the w_{QS} from this relation, which is in turn used to derive the final width w_{QC}.

The equations described thus far are only valid for weakly coupled plasmas. For plasmas with strong coupling, the ion microfield deviates from the Holtsmark distribution significantly, and we therefore introduce a correction factor such that $w = w_{QC}\eta$ and determine η as

$$\eta = \frac{w_{QS}^S}{w_{QS}^H}, \qquad (16)$$

where w_{QS}^S is the quasistatic width calculated with a realistic ion microfield distribution for a strongly coupled plasma, while w_{QS}^H is calculated with the Holtsmark distribution. We use the fitting formula of the ion field distribution from Potekhin *et al.* [19] to compute this correction factor. The fitting formula for the field distribution depends on two parameters, the ion-ion coupling parameter

$$\Gamma = \frac{z_i^2 e^2}{kTR_s} \qquad (17)$$

and the electron screening parameter

$$s = \frac{R_s}{R_d}, \qquad (18)$$

TABLE I. Parameters for the normalized coupling and screening parameters in Eq. (21).

s range	a_0	a_1	a_2	a_3	a_4	a_5	a_6	a_7	a_8	a_9
$0.0 \leqslant s \leqslant 1.0$	0.0000	0.9779	1.2651	1.2226	-0.2520	0.1508	-0.1970	0.0839	1.1811	1.1901
$1.0 < s \leqslant 1.5$	0.5639	0.9400	1.2475	1.2270	-0.1961	0.1490	-0.0844	0.0614	1.1317	1.0023
$1.5 < s \leqslant 2.0$	1.0422	0.9344	1.2318	1.6241	-0.08178	0.1699	0.01409	-0.0242	0.1494	0.2670
$2.0 < s \leqslant 2.5$	1.1156	0.2383	1.2864	5.0000	-0.0323	0.6368	0.09548	-0.1263	0.0265	0.0224
$2.5 < s \leqslant 3.0$	0.7558	0.9654	1.2286	0.8245	-0.1402	0.0322	0.0140	0.2465	0.9557	0.1263

such that

$$P(F) = \tilde{P}(\beta, \Gamma, s), \tag{19}$$

where $\beta = F/F_0$, and $F_0 = \frac{z_i e}{R_i^2}$ is the normal field strength.

One drawback of the fitting formula in Potekhin *et al.* [19] is that for a charged radiator it is assumed that the radiator and perturber charges are the same. However, in many situations, the radiator is a minority dopant in a plasma with different perturber ion charges. To account for this, we used a version of the adjustable parameter exponential approximation (APEX) code to compute the ion field distribution for different radiator-perturber charge ratios $z_{ri} = z_r/z_i$, and to numerically fit the field distribution in terms of $\tilde{P}(\beta, \Gamma, s)$ of Potekhin *et al.* [19] as

$$\tilde{W}(\beta, \Gamma, s, z_{ri}) = \tilde{P}(\beta, \Gamma_n, s_n), \tag{20}$$

where the normalized coupling parameter Γ_n and screening parameter s_n are determined as

$$\Gamma_0 = a_8 \Gamma, \quad z_0 = a_9 z_{ri}, \quad g_0 = \frac{a_0 + a_1 z_0}{1 + z_0},$$
$$g_1 = \frac{a_2 + a_3 z_0}{1 + z_0}, \quad s_0 = \frac{a_4 + a_5 z_0}{1 + z_0}, \quad s_1 = \frac{a_6 + a_7 z_0}{1 + z_0},$$
$$p_0 = \frac{g_0 + g_1 \Gamma_0}{1 + \Gamma_0}, \quad p_1 = \frac{s_0 + s_1 \Gamma_0}{1 + \Gamma_0}, \quad \Gamma_n = \Gamma z_{ri}^{p_0},$$
$$s_n = s z_{ri}^{p_1}. \tag{21}$$

The parameters a_0 through a_9 are determined from the numerical fit in five intervals of s as given in Table I.

To demonstrate the quality of our fits to the field distributions, we show two examples. Figure 3 shows the field distributions calculated with APEX and the fit formula for $z_r = 18$, $z_i = 18$, $s = 1.0$, and $\Gamma = 6.0$. In this case, we have $z_r = z_i$, so that no normalization of the screening and coupling parameters is needed. Figure 4 shows the field distributions calculated with APEX and the fit formula for $z_r = 18$, $z_i = 2$, $s = 1.0$, and $\Gamma = 0.67$. The normalized screening and coupling parameters for this case are $s_n = 1.22$ and $\Gamma_n = 6.56$. The fitted distributions using both the normalized and original parameters are shown. The fit with the original parameters corresponds to the case with $z_i = z_r = 2$. It is clear that the formula using normalized screening and coupling parameters reproduces the APEX field distribution much better.

Finally, to deal with plasmas with multiple ionic perturbers, we first determine the ion contributions to the width as

$$w^i = \sum_k c_k w_k, \tag{22}$$

where c_k is the weight of ionic species k by number, and w_k is the width of the species k calculated as if it is the only ion in

the plasma. The total Stark width is then the sum of electron and ion contributions: $w^t = w^i + w^e$. Strictly speaking, such a procedure to account for multiple plasma particle species is only valid in the impact approximation, when the density dependence of all component widths is linear. Other types of summation schemes are also in widespread use; e.g., Stambulchik and Maron [18] propose

$$w = \left(\sum_k w_k^{3/2} \right)^{2/3}, \tag{23}$$

which is valid when the widths of all components can be described by the quasistatic approximation. However, the broadening due to different plasma components may have different density dependences in general, and since our objective here is to provide an efficient method suitable for use in large scale collisional radiative models, such that minor loss of accuracy can be tolerated, we choose the simpler linear weighting scheme.

The procedure thus outlined contains an empirical parameter, R_0. A value of 0.5 is suggested in Stambulchik and Maron [18]. However, this depends on the particular choice of the quasistatic width formula. In our case, we choose $R_0 = 2$, so that the calculated width of the H-like Ar Lyβ transition matches that of Keane *et al.* [22] at a temperature of 1 keV when the Ar ion is a minor dopant in a fully ionized deuterium plasma, as shown in Fig. 5.
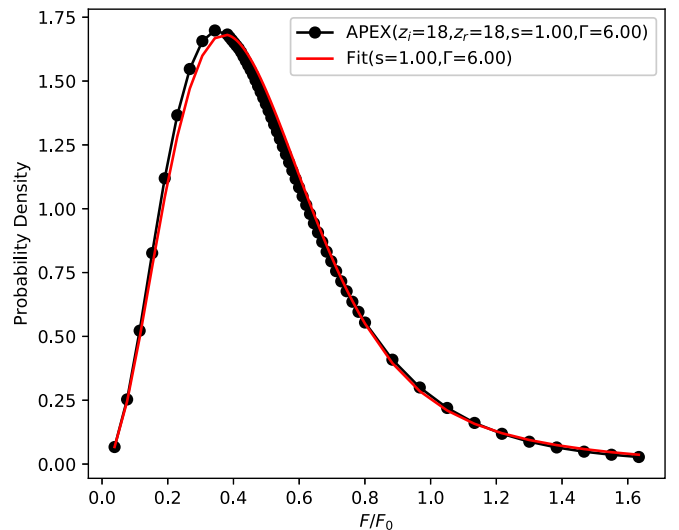

FIG. 3. Ion microfield distributions calculated with APEX and the numerical fit formula for $z_r = 18$, $z_i = 18$, $s = 1.0$, and $\Gamma = 6.0$.
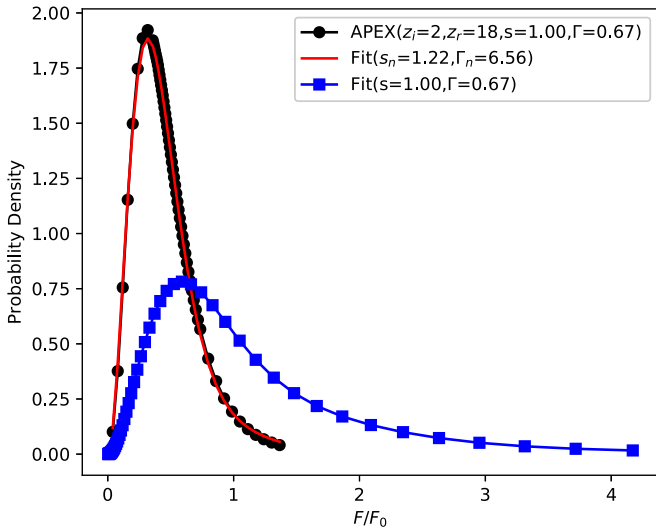
FIG. 4. Ion microfield distributions calculated with APEX and the numerical fit formula for $z_r = 18$, $z_i = 2$, $s = 1.0$, and $\Gamma = 0.67$. The fitted results from original screening and coupling parameters and from normalized ones ($s_n = 1.22$ and $\Gamma_n = 6.56$) are both shown.

IV. COMPARISON BETWEEN THEORY AND EXPERIMENT FOR THE $K\beta$ TRANSITION OF He-LIKE Cl

Recently, the Stark shifts and widths of the $K\beta$ transition of He-like Cl have been measured with a high-resolution crystal spectrometer on the Orion laser facility [12]. The targets used were PyD and KCl. The temperatures of the plasmas were estimated to be about 600–650 eV. The electron densities were inferred from the Stark width using its calculated density dependence assuming He-like Cl ions are embedded in a KCl plasma and at a temperature of 600 eV. The experimentally determined density dependence of the shifts were then compared with the theoretical results of Li and Rosmej [13]. It was shown that the theoretical curve lies significantly higher than the measured one.

Using the methods described in the previous sections, we have calculated the density dependence of both shifts and widths of the $K\beta$ transition of He-like Cl for three different plasmas at a temperature of 625 eV: fully ionized deuterium;
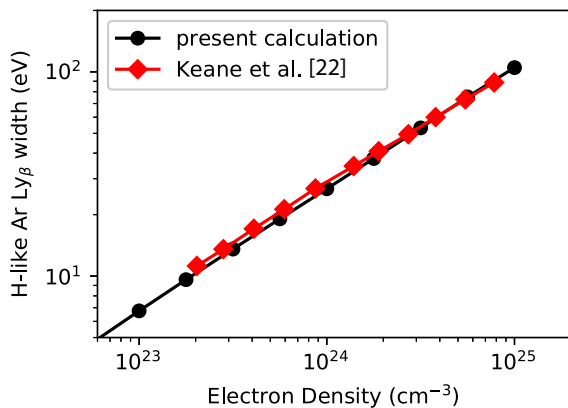

FIG. 5. Stark width of the Lyβ transition of H-like Ar at a temperature of 1 keV, and embedded in a fully ionized deuterium plasma. The empirical constant R_0 is 2 in the present calculation in order to match the data from [22].
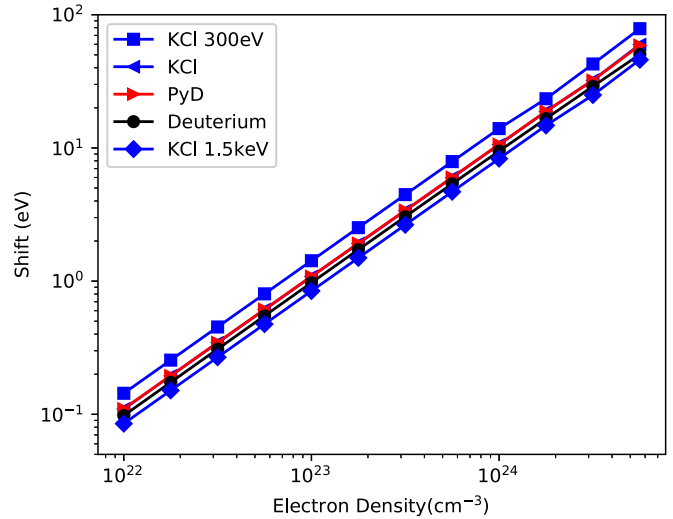

FIG. 6. The calculated density dependence of the shifts of the $K\beta$ transition of He-like Cl in different target plasmas at a temperature of 625 eV. For the KCl target, the results at two additional temperatures of 300 eV and 1.5 keV are also shown. The ordering of the legends coincides with that of the curves at the low density end. Note that the shifts for KCl and PyD plasmas at 625 eV nearly overlap, and the curve for the deuterium plasma is just slightly below them.

PyD ($C_{16}H_{12}Cl_4$), in which C and H are fully ionized, while Cl is assumed to be in the He-like charge state; and KCl, where both the K and Cl ions are in the He-like charge state. For the KCl target, we also made calculations at two additional temperatures, 300 eV and 1.5 keV. The results are shown in Figs. 6 and 7. It is seen that the target plasma dependence of the energy shift is minimal, while that of the width is more pronounced. The width calculation used to determine densities in Beiersdorfer *et al.* [12] is shown to be close to the present results for a PyD plasma at densities below
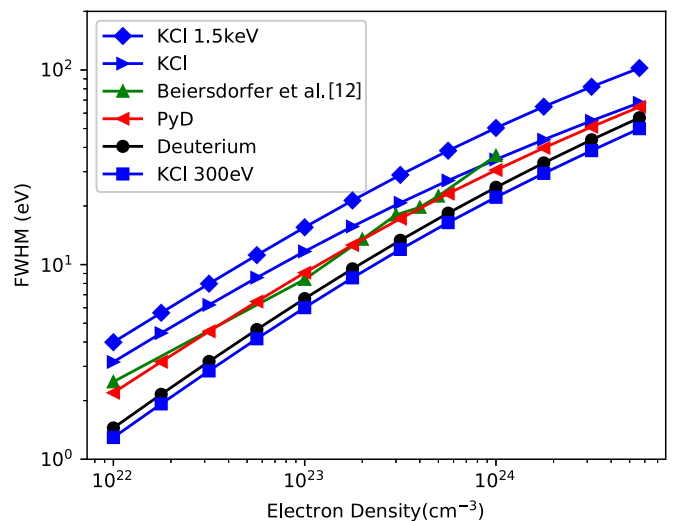

FIG. 7. The calculated density dependence of the widths of the $K\beta$ transition of He-like Cl in different target plasmas at a temperature of 625 eV, and for the KCl target, at two additional temperatures of 300 eV and 1.5 keV. The width-density relation used in Beiersdorfer *et al.* [12] is also shown for comparison. The ordering of the legends coincides with that of the curves at the low density end.
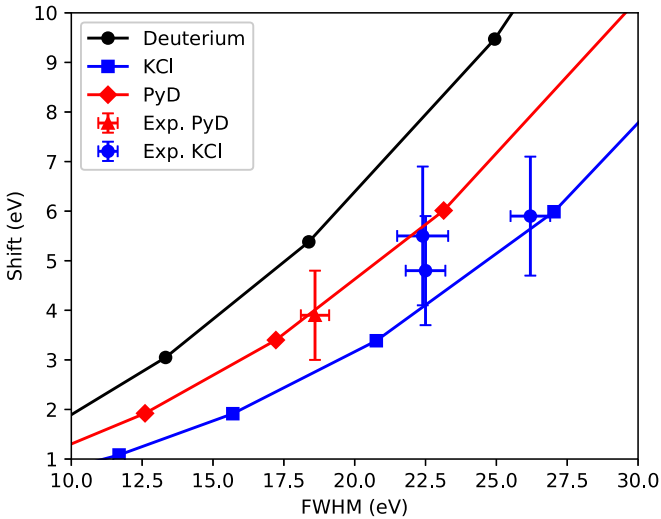
FIG. 8. The measured shift-width relation of $K\beta$ transition of He-like Cl, and comparison with theoretical results for different target plasma compositions at a temperature of 625 eV.

2×10^{23} cm^{-3}, but becomes closer to the present KCl plasma widths at higher densities.

Since the experiment measured the shifts and widths directly instead of densities, we therefore make a detailed comparison of the shift-width relationship between the measurement and the calculated ones for different targets. The results are shown in Fig. 8. We show three theoretical shift-width relations for deuterium, PyD, and KCl targets at a temperature of 625 eV, respectively. It is seen that the measurements agree better with the calculations using the appropriate target plasmas.

V. CONCLUSION

In conclusion, we have developed numerical models of field induced line shifts and broadening of complex ions embedded in warm dense plasmas. The resulting shift and width of the He-like Cl $K\beta$ transition agree well with the recent measurements from the Orion laser facility. Our calculations strongly suggest that it is advantageous to employ line-shift measurements as a diagnostic for the electron density of high-density plasmas. Using line-shift measurements to determine the plasma density is especially attractive in light of our past experiences with linewidth measurements, which can be hampered by line asymmetries and uncertainties in determining the proper background levels. By contrast, the center position of a line is rather well defined—in the case of the He-like Cl $K\beta$ line its position is defined by its central dip. Moreover, our calculations show that, unlike the linewidth, a given line shift is only weakly dependent on the plasma composition, as shown in Figs. 6 and 7. Similarly, the dependence on the electron temperature is also much weaker for the line shift than for the linewidth. This weak dependence greatly reduces the uncertainties associated with an experimentally inferred density. The good agreement between our calculations and the measurements shown in Fig. 8 gives us confidence that our calculations can be reliably used to employ line-shift measurements for determining the electron density.

[1] D. R. Inglis and E. Teller, Astrophys. J. **90**, 439 (1939).

[2] H. R. Griem, J. Phys. **49**, C1 (1988).

[3] A. Saemann, K. Eidmann, I. E. Golovkin, R. C. Mancini, E. Andersson, E. Förster, and K. Witte, Phys. Rev. Lett. **82**, 4843 (1999).

[4] O. Ciricosta, S. M. Vinko, H. K. Chung, B. I. Cho, C. R. D. Brown, T. Burian, J. Chalupský, K. Engelhorn, R. W. Falcone, C. Graves *et al.*, Phys. Rev. Lett. **109**, 065002 (2012).

[5] D. J. Hoarty, P. Allan, S. F. James, C. R. D. Brown, L. M. R. Hobbs, M. P. Hill, J. W. O. Harris, J. Morton, M. G. Brookes, R. Shepherd *et al.*, Phys. Rev. Lett. **110**, 265003 (2013).

[6] S. B. Hansen, E. C. Harding, P. F. Knapp, M. R. Gomez, T. Nagayama, and J. E. Bailey, High Energy Density Phys. **24**, 39 (2017).

[7] J. Deprince, M. A. Bautista, S. Fritzsche, J. A. García, T. R. Kallman, C. Mendoza, P. Palmeri, and P. Quinet, Astron. Astrophys. **624**, A74 (2019).

[8] J. Deprince, M. A. Bautista, S. Fritzsche, J. A. García, T. Kallman, C. Mendoza, P. Palmeri, and P. Quinet, Astron. Astrophys. **626**, A83 (2019).

[9] B. A. Hammel, C. J. Keane, M. D. Cable, D. R. Kania, J. D. Kilkenny, R. W. Lee, and R. Pasha, Phys. Rev. Lett. **70**, 1263 (1993).

[10] N. C. Woolsey, C. A. Back, R. W. Lee, A. Calisti, C. Mossé, R. Stamm, B. Talin, A. Asfaw, and L. S. Klein, J. Quant. Spectrosc. Radiat. Transfer **65**, 573 (2000).

[11] P. Beiersdorfer, G. V. Brown, R. Shepherd, P. Allan, C. R. D. Brown, M. P. Hill, D. J. Hoarty, L. M. R. Hobbs, S. F. James, H. K. Chung *et al.*, Phys. Plasmas **23**, 101211 (2016).

[12] P. Beiersdorfer, G. V. Brown, A. McKelvey, R. Shepherd, D. J. Hoarty, C. R. D. Brown, M. P. Hill, L. M. R. Hobbs, S. F. James, J. Morton *et al.*, Phys. Rev. A **100**, 012511 (2019).

[13] X. Li and F. B. Rosmej, Europhys. Lett. **99**, 33001 (2012).

[14] M. F. Gu, Can. J. Phys. **86**, 675 (2008).

[15] M. Belkhiri and M. Poirier, Phys. Rev. A **90**, 062712 (2014).

[16] M. Belkhiri and M. Poirier, High Energy Density Phys. **9**, 609 (2013).

[17] J. C. Stewart and K. D. Pyatt, Jr., Astrophys. J. **144**, 1203 (1966).

[18] E. Stambulchik and Y. Maron, J. Phys. B **41**, 095703 (2008).

[19] A. Y. Potekhin, G. Chabrier, and D. Gilles, Phys. Rev. E **65**, 036412 (2002).

[20] Y. Li, J. Wu, Y. Hou, and J. Yuan, J. Phys. B **41**, 145002 (2008).

[21] M. Baranger, Phys. Rev. **112**, 855 (1958).

[22] C. J. Keane, B. A. Hammel, D. R. Kania, J. D. Kilkenny, R. W. Lee, A. L. Osterheld, L. J. Suter, R. C. Mancini, C. F. Hooper Jr., and N. D. Delamater, Phys. Fluids B **5**, 3328 (1993).